Metalurgi (2024) 1: 49 - 62

METALURGI
Majalah Ilmu dan Teknologi
p-ISSN 0126-3188 | e-ISSN 2443-3926
ejurnalmaterialmetalurgi.lipi.go.id

MICROSTRUCTURAL STABILITY AND HIGH-TEMPERATURE OXIDATION BEHAVIOR OF $Al_{0.25}$CoCrCuFeNi HIGH ENTROPY ALLOY

Fadhli Muhammad[a,*], Ernyta Mei Lestari[a], Tria Laksana Achmad[a], Akhmad Ardian Korda[a], Budi Prawara[b], Djoko Hadi Prajitno[c], Bagus Hayatul Jihad[d], Muhamad Hananuputra Setianto[d], and Eddy Agus Basuki[a]

[a]Department of Metallurgical Engineering, Institut Teknologi Bandung
Jl. Ganesha No. 10, Bandung, Indonesia 40132
[b]Research Centre for Advanced Materials, National Research and Innovation Agency
Jl. Sangkuriang, Bandung, Indonesia 40135
[c]Research Organization for Nuclear Technology, National Research and Innovation Agency
Jl. Tamansari No. 71, Bandung, Indonesia 40132
[d]Research Center for Rocket Technology, National Research and Innovation Agency
Jalan Raya Lapan, Parungpanjang, Kabupaten Bogor, Indonesia 16350
*E-mail: fadhlim_08@itb.ac.id

Received: 26-01-2024, Revised: 23-08-2024, Accepted: 12-09-2024

Abstract

$Al_{0.25}$CoCrCuFeNi is a high-entropy alloy composed of transition metals, specifically designed for high-temperature applications owing to its favorable mechanical properties, high melting point, and excellent high-temperature resistance. This alloy has been identified as a promising material for space exploration, particularly in the fabrication of combustion chambers and rocket nozzles by the National Aeronautics and Space Agency. Ongoing alloy development involves modifying the elemental composition. This study reduced aluminum content in the equiatomic AlCoCrCuFeNi alloy to $Al_{0.25}$CoCrCuFeNi, followed by isothermal oxidation treatments at 800, 900, and 1000°C. A series of experiments were conducted to investigate the microstructure stability and oxidation behavior of the $Al_{0.25}$CoCrCuFeNi alloy. The alloying elements were melted using a single DC electric arc furnace, followed by homogenization at 1100°C for 10 hours in an inert atmosphere. Subsequently, samples were cut into coupons for isothermal oxidation testing at the desired temperatures for 2, 16, 40, and 168 hours. The oxidized samples were characterized using XRD (x-ray diffraction), SEM (scanning electron microscopy) equipped with EDS (energy-dispersive X-ray spectroscopy), optical microscopy, and Vickers hardness testing. The as-homogenized alloy consisted of two constituent phases: an FCC (face-centered cubic) phase in the dendritic region and a copper-rich FCC phase in the inter-dendritic region. The oxides formed during the oxidation process included Al_2O_3, Cr_2O_3, Fe_3O_4, CoO, CuO, NiO, and spinel oxides (Co, Ni, Cu)(Al, Cr, Fe)$_2$ O_4), with distinct formation mechanisms at each temperature.

Keywords: *High-entropy alloy, isothermal oxidation, FCC structure, high temperature, phase stability*

1. INTRODUCTION

Equipment and machinery employed in high-temperature applications, including rocket nozzles, nuclear reactor piping systems, aircraft and power plant gas turbine blades, power plant boilers, steam turbines, and combustion engine exhaust facilities, necessitate materials capable of enduring elevated temperatures. These components demand properties essential for operation in environments characterized by high temperatures, stresses, pressures, and exposure to oxidative and corrosive conditions.

Nickel-based superalloys were traditionally considered the most suitable materials for high-temperature applications [1]-[3]. However, these alloys have now reached their operational temperature limits. A γ'-Ni_3Al is an ordered, coherent precipitate that significantly strengthens nickel-based superalloys. When the temperature exceeds their γ-NiAl/γ'-Ni_3Al equilibrium solvus temperature, complete dissolution of the γ'

DOI : 10.55981/metalurgi.2024.745

Metalurgi is Sinta 2 Journal (https://sinta.kemdikbud.go.id/journals/profile/3708) accredited by Ministry of Education, Culture, Research, and Technology, Republic Indonesia

precipitate occurs, leading to a relatively weak γ solid solution matrix [4]-[5].

Among numerous potential materials, HEAs (high entropy alloys) offer a promising solution to the challenge of balancing high-temperature strength with oxidation and corrosion resistance. HEAs differ from conventional alloys by having equal molar concentrations of each constituent element [6]. These alloys exhibit four primary effects: high entropy, lattice distortion, sluggish diffusion, and the cocktail effect. The cocktail effect allows for tailoring alloy properties through adjustments in elemental composition [7].

HEAs also referred to as multi-component alloys, have been developed specifically for high-temperature applications. This category includes refractory high entropy alloys (RHEAs) and transition metal high entropy alloys (TM-HEAs). RHEAs, such as VNbMoTaW, MoNbTaW, and CrMoTaNb, are renowned for their exceptional mechanical properties [8]. However, they can be brittle and costly due to the use of refractory elements. TM-HEAs are composed of more affordable elements, including Fe, Al, Co, Ni, Cu, Ti, and Cr [9]. Some elements, such as FeNi, Cu, and Al, have also been produced in Indonesia.
HEA composed of transition metals, such as AlCoCrFeNi, AlCoCrCuFeNi, and CoCrFeNiTi [6], have been extensively studied. Lu et al. [10] observed that a decreased diffusion rate of aluminum in AlCoCrFeNi alloys leads to a lower oxidation rate, thereby improving their oxidation resistance. Butler et al. [11]-[12] evaluated the influence of aluminum content on the oxidation behavior of as-cast AlxCoCrFeNi at 1050°C. They determined that alloys with relatively low aluminum levels developed discontinuous chromium oxide (Cr2O3) layers on the outer surface and internal aluminum oxide (Al_2O_3) scales. Conversely, alloys with higher aluminum concentrations developed a continuous Al_2O_3 layer. However, due to its high aluminum content, the equiatomic AlCoCrCuFeNi often exhibits brittle behavior. The study sought to reduce the aluminum content of the equiatomic AlCoCrCuFeNialloy to $Al_{0.25}$CoCrCuFeNi. The objective was to evaluate the impact of this reduction on the alloy's isothermal oxidation resistance, microstructure stability, and hardness.

2. MATERIALS AND METHODS

A vacuum arc furnace produced the high entropy alloy with a nominal composition of Al0.25CoCrCuFeNi under an argon atmosphere on a water-cooled copper mold. The purity of each element metal was more than 99.7 wt.%. The ingots were flipped and re-melted at least five times to ensure the homogeneous composition obtained. The homogenization was further carried out using a horizontal tube furnace under an argon atmosphere with a flow of 10 mL/min for 10 h at 1100 °C. Specimens with dimensions of approximately 7.5 mm x 4 mm x 2 mm were extracted from the ingots for the oxidation test. The specimens were oxidized at 800, 900, and 1000 °C in laboratory air, with 2, 16, and 40 h exposure times for each temperature. An extended oxidation test for 168 h was conducted at 1000 °C to observe oxidation behavior further. Isothermal oxidation tests were performed in a horizontal tube furnace in which both ends of the tube opened and can achieve a maximum working temperature of around 1200 °C.

During oxidation tests, specimens were placed in alumina boats and positioned in the heating zone once the target temperature was reached. They were then removed from the furnace and allowed to cool in the air once the oxidation tests were completed. One specimen was used for each oxidation test. After each oxidation test, the sample was weighed using an analytical balance with an accuracy of 0.1 mg.
The phase constitution of the oxidized sample and oxidation product were characterized by XRD (x-ray diffraction) SmartLab, Rigaku using Cu-Kα radiation (λ=0.154 nm) functioning at 40 kV. Microstructure and chemical composition were studied using an optical microscope and SEM (scanning electron microscope) JCM-7000 NeoScope™, JEOL equipped with an EDS (energy dispersive spectrometer).The cross-section surface was subject to mechanical polishing but not etching. The Vickers hardness test was conducted on a polished cross-sectional surface using a diamond pyramid indentation undera 98.07 N load applied for 20 s. Five indentations were measured to obtain an average value of each sample.

3. RESULTS AND DISCUSSION

3.1 Microstructure Analysis and Hardness of $Al_{0.25}$CoCrCuFeNi

Previous studies [13]-[14] have reported that the $Al_{0.3}$CoCrCuFeNi alloy consists of a DR (dendritic region) with an FCC (face-centered cubic) microstructure and an inter-dendritic region (ID) with Cu-rich FCC microstructure. Butler, et al. [11] also investigated the oxidation behavior of $Al_x(CoCrFeNi)_{100-x}$ alloy (x = 8, 10, 12, 15, 20, 30 at.%) and confirmed that the microstructure of high entropy alloy with low Al content is FCC, whereas those with high Al

content exhibit a BCC (body-centered cubic) structure.

According to the phase diagram constructed by Turchi et al. [1], the $Al_{0.25}CoCrCuFeNi$ alloy exists in equilibrium with the FCC phase and a Cu-rich FCC phase at 800, 900, and 1000 ℃. To predict the crystal structure of the alloy, the VEC (valence electron concentration) was calculated. A VEC of 8.52 for $Al_{0.25}CoCrCuFeNi$ indicates the stability of the FCC structure [13]. Other thermodynamic parameters, including the entropy of mixing (ΔS_{mix}), enthalpy of mixing (ΔH_{mix}), atomic size mismatch (δ), and mixing parameter (Ω), were also calculated and found to be 14.34 $JK^{-1}mol^{-1}$, 0.62 $kJmol^{-1}$, 3.18%, and 40.19, respectively.

As illustrated in Fig. 1, the microstructure reveals that the dark-colored inter-dendritic region exhibits a Cu-rich FCC structure, while the bright-colored dendritic region possesses an FCC structure. According to Table 1, the inter-dendritic section contains the highest concentration of copper at 63.91 at.% as determined by EDS. The segregation of copper in the inter-dendritic regions can be attributed to the bonding energy between copper and other elements. Copper exhibits a positive enthalpy of mixing with cobalt, chromium, iron, and nickel, which are 6, 12, 13, and 4 kJ/mol, respectively [14].

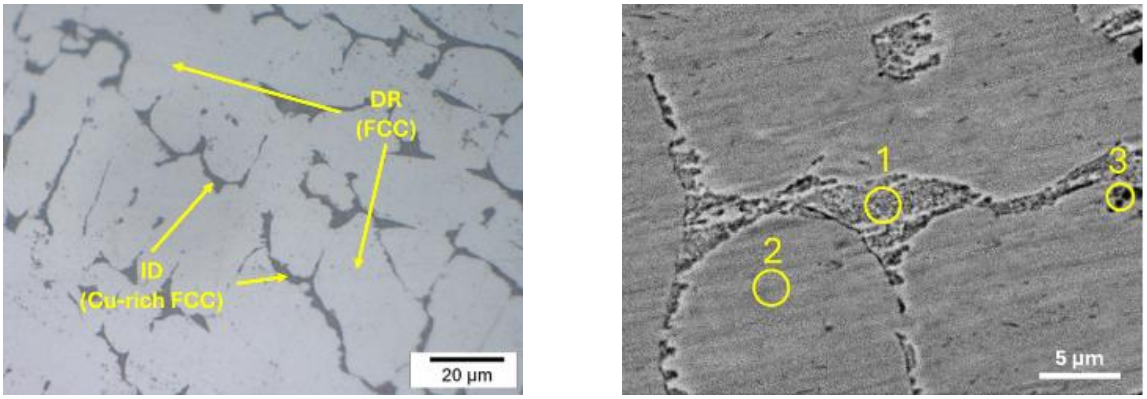

(a) (b)

Figure 1. Microstructure of *as-homogenized* $Al_{0.25}CoCrCuFeNi$alloy. (a) Optical microscope showing dendritic and inter-dendritic areas at high magnification, (b) Backscattered electron image showing dendritic and inter-dendritic areas. Point 1-3 indicate EDS point analysis

This suggests that copper tends to avoid bonding preferentially with the dendrite part, which is enriched in cobalt, chromium, iron, and nickel. Table 1 further demonstrates that the inter-dendritic region exhibits a higher aluminum content than the initial composition, while the copper in the dendritic region displays a lower concentration of approximately 9.89% compared to the initial composition of 19.05%.

Table 1. Chemical composition of *as-homogenized*$Al_{0.25}CoCrCuFeNi$ obtained from EDS point analysis

Point	**Elements (at.%)**					
	Al	**Co**	**Cr**	**Cu**	**Fe**	**Ni**
1	10.56	3.19	1.51	63.91	2.76	18.07
2	5.69	22.56	21.54	9.89	21.34	20.34
3	16.30	21.20	18.50	11.83	17.57	17.78

Figure 2 illustrates the average hardness values of the *as-homogenized* $Al_{0.25}CoCrCuFeNi$. The hardness test results indicate a general trend of decreasing hardness with increasing exposure time.

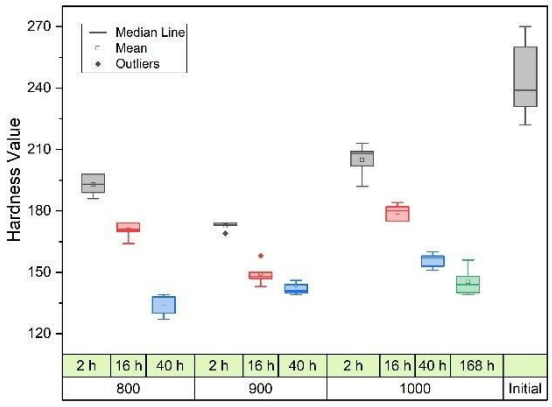

Figure 2. The hardness value of the $Al_{0.25}CoCrCuFeNi$ alloy at various temperatures as a function of exposure time. (Initial means *as-homogenized* alloy)

This decrease in hardness is attributed to the reduced Al content, which becomes concentrated at the substrate due to the diffusion of Al atoms to the metal/oxide interface to form a protective Al_2O_3 layer. During oxidation, Al is consumed to

create this protective layer, resulting in a concentration gradient that drives the diffusion of Al atoms from the substrate to the surface. Aluminum has a larger atomic radius (143 pm) than the other alloying elements (ranging from 124 to 128 pm). Consequently, a decrease in Al content leads to a reduction in lattice distortion within the alloy [15].

3.2 Oxidation Kinetic

Figure 3 presents the specific weight gain of the $Al_{0.25}CoCrCuFeNi$ alloy during isothermal oxidation testing within the 800-1000 °C temperature range. At 800 and 900 °C, no substantial weight gain was observed, and the oxidation profile exhibited steady growth. However, at 1000 °C, a significant increase in weight gain was noted after 40 h of oxidation, suggesting a rapid oxidation rate.

During the initial stages of oxidation, an astable oxide scale was observed for up to 16 hat all oxidation temperatures. However, the alloy demonstrated a sudden increase in oxidation rate after prolonged exposure at 1000 °C, resulting in rapid oxidation. To gain further insights into its oxidation behavior, the oxidation test was extended to 168 h, revealing a semi-parabolic oxidation profile.

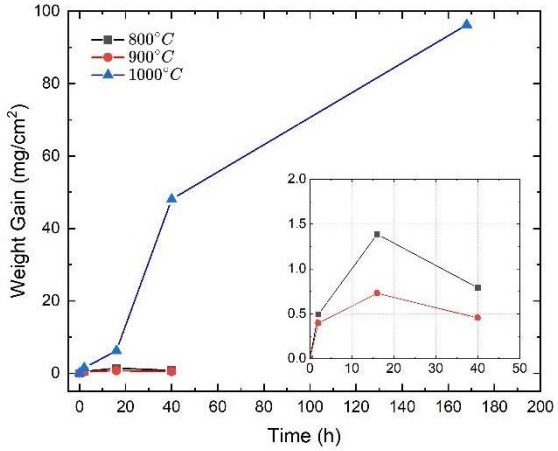

Figure 3. Oxidation weight gain of the $Al_{0.25}CoCrCuFeNi$ alloy at 800-1000 °C

In summary, the oxidation resistance of the $Al_{0.25}CoCrCuFeNi$ is strongly influenced by temperature and time. However, the primary objective of this study is to elucidate the oxidation mechanism and morphology of the formed oxides, rather than delving into detailed information on oxidation kinetics, such as the oxidation rate.

3.3 Oxide Scale Morphology

Figure 4 presents the XRD diffractogram of the alloy at 800-1000 °C. The diffractogram patterns indicate the formation of Al_2O_3, Cr_2O_3, NiO, CoO, Fe_3O_4, CuO, and spinel. All types ofAl_2O_3formed were transient oxides, with variations such as γ-Al_2O_3, δ-Al_2O_3, and θ-Al_2O_3 at 800, 900, and 1000°C, respectively. However, these transient oxides exhibit poor oxidation resistance [16]. Additionally, an alloy substrate consisting of FCC and Cu-rich FCC phases was detected at all temperature ranges.

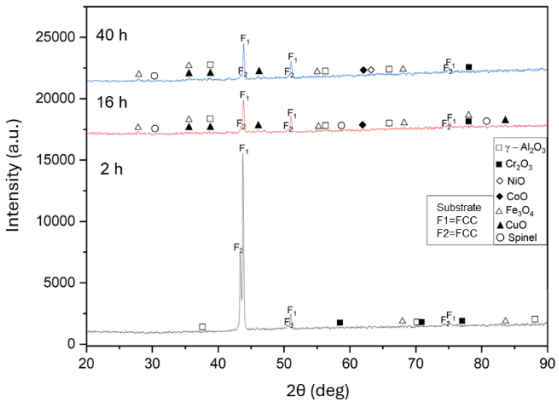

(a)

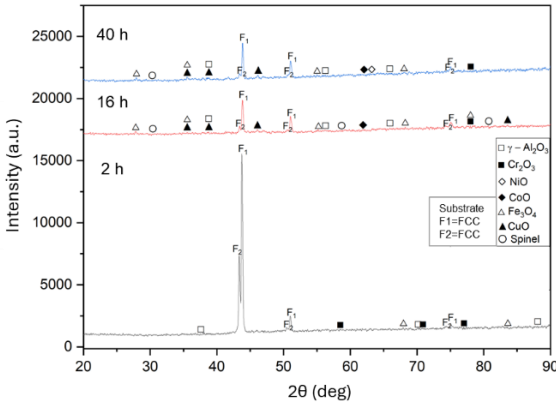

(b)

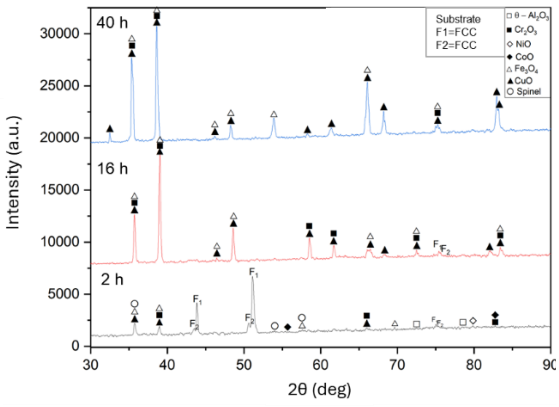

(c)

Figure 4. The XRD diffractogram of the $Al_{0.25}CoCrCuFeNi$ alloy at (a) 800 °C, (b) 900 °C, (c) 1000 °C

Figures 5-7 illustrate the morphology of the oxide layer formed on the surface of $Al_{0.25}CoCuCrFeNi$ for samples held at 800, 900, and 1000 °C for 40 h, as well as samples held at

1000 ℃ for 168 h in Fig. 8. The composition of the formed oxides in Fig. 5(a), as presented in Table 2, is predominantly composed of Cu and Cr, with respective compositions of 23.03 at% and 14.38 at.%.

Figure 5(b) depicts the oxide morphology, which is dominated by Al, followed by Cr with a composition of 33.83 at.% and 8.12 at.%, respectively. In Figure 5(c), the morphological image reveals a small plate-like shape of a spinel oxide composed of Al-Cr-Cu-Fe.

Table 2. Chemical composition of oxidized sample at 800 °C for 40 h according to EDS point analysis in Figure 5

Point	Elements (at.%)						
	Al	Co	Cr	Cu	Fe	Ni	O
1	1.56	4.22	14.38	23.03	2.15	1.58	53.07
2	33.83	2.44	8.12	2.11	3.24	2.44	48.29
3	17.23	3.40	13.00	9.08	10.34	2.69	44.27

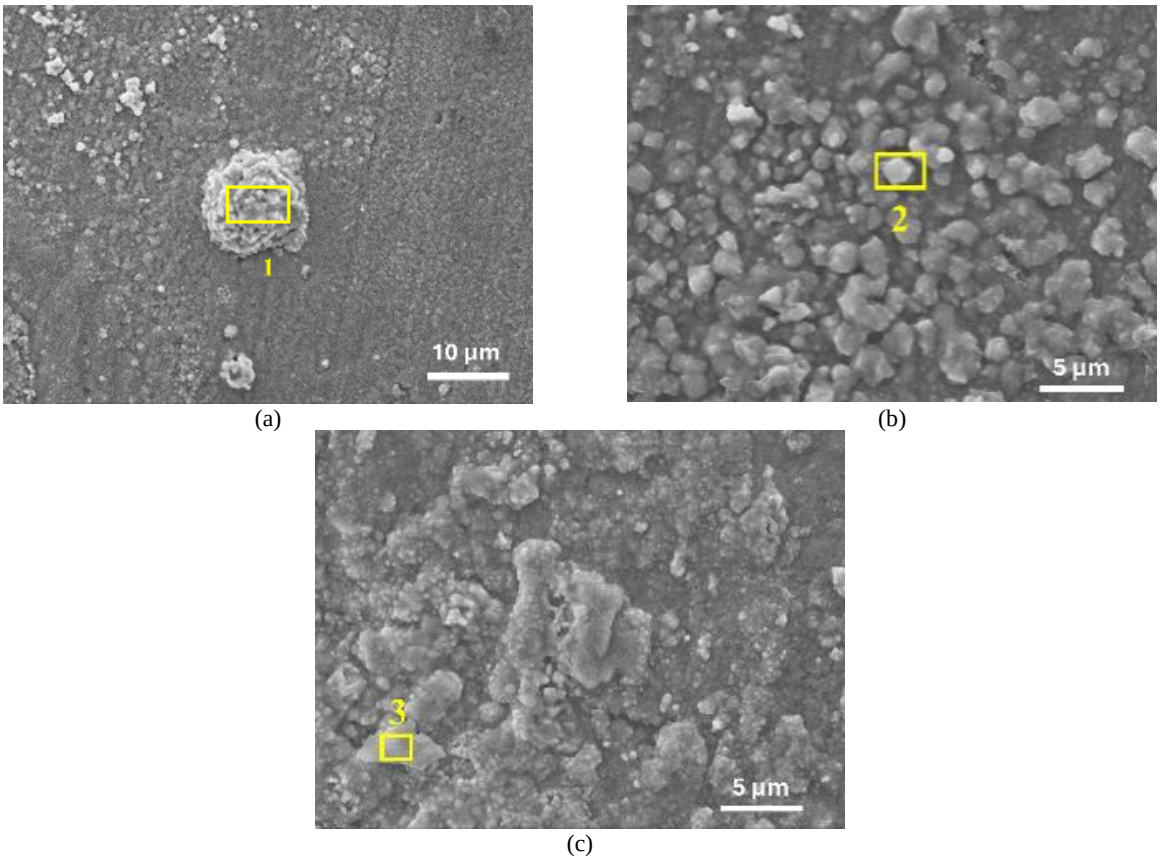

(a) (b) (c)

Figure 5. Surface morphology of sample at 800 °C for 40 h

In the sample oxidized at 900 ℃ for 40 h, a thin oxide layer formed on the surface. SEM analysis revealed that certain portions of the oxide had peeled off, as illustrated in Figs. 6(a) and 6(c).

The composition of these peeled-off sections corresponds to $Al_{0.25}CoCrCuFeNi$, except Cu (see Table 3). Figure 6(b) depicts a thin plate-like structure with Al as the dominant element, indicating the formation of Al_2O_3 oxide.

Table 3. Chemical composition of oxidized sample at 900 °C for 40 h according to EDS point analysis in Figure 6

Point	Elements (at.%)						
	Al	Co	Cr	Cu	Fe	Ni	O
1	31.72	0.48	1.59	1.06	0.35	0.43	64.37
2	4.20	21.79	21.99	5.26	21.48	19.78	5.50

The outermost oxide layer formed on the surface of the samples oxidized at 1000 ℃ for 40 h and 168h is predominantly composed of Cu.

Table 4. Chemical composition of oxidized sample at 1000 °C for 40 h according to EDS point analysis in Figure 7

Point	Elements (at.%)						
	Al	Co	Cr	Cu	Fe	Ni	O
1	2.29	0.50	0.56	39.78	0.28	0.87	55.72
2	0.70	1.15	-	54.51	0.04	0.04	43.56
3	0.15	1.31	0.08	49.64	0.08	0.64	48.10

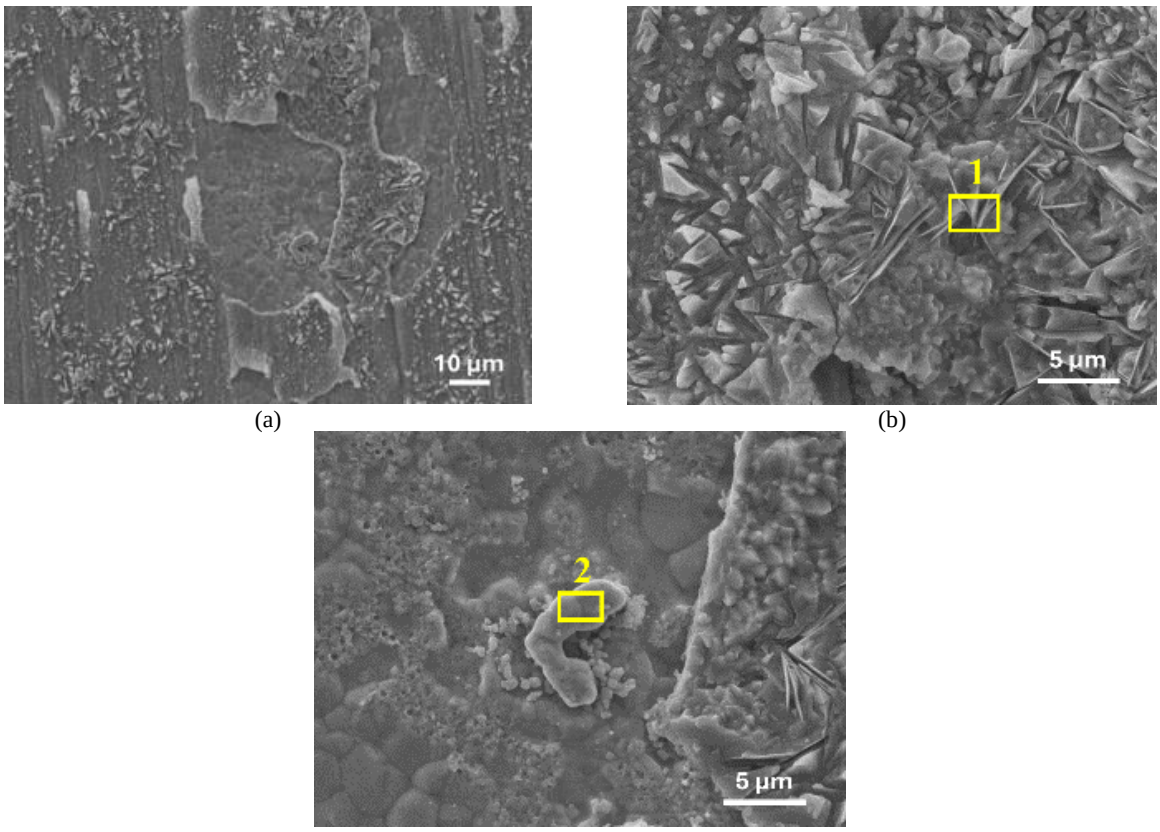

(a) (b) (c)

Figure 6. Surface morphology of sample at 900 °C for 40 h

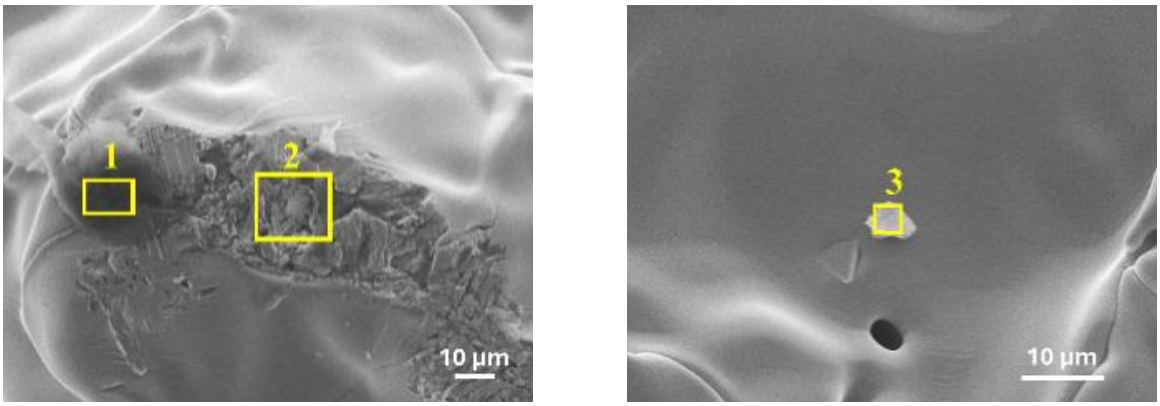

(a) (b)

Figure 7. Surface morphology of sample at 1000 °C for 40 h

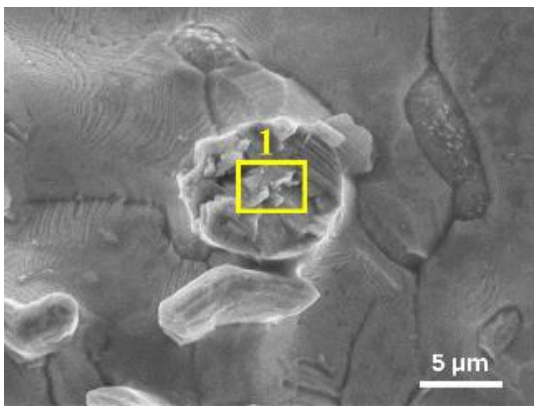

Figure 8. Surface morphology of sample at 1000 °C for 168 h

EDS point analysis of Figs. 7 and 8 indicate that the outermost oxide layer is dominated by Cu, as shown in Tables 4 and 5. The resulting CuO oxide layer exhibits a dense and non-porous structure.

Table 5. Chemical composition of oxidized sample at 1000 °C for 168 h according to EDS point analysis in Figure 8

Point	Elements (at.%)						
	Al	Co	Cr	Cu	Fe	Ni	O
1	0.05	2.35	-	42.08	0.13	1.61	53.78

3.4 Cross-section Analysis

Figures 9-11 depict the X-ray mapping of the alloy cross section after oxidation testing at 800, 900, and 1000 ℃ for 2 h. At 800 ℃, a thin oxide layer dominated by Al and Cr formed on the sample surface, as shown in Fig. 9. Meanwhile, the oxide layer at 900 ℃ is composed of a mixture of elements, including Al, Co, Cr, Cu, Fe, and Ni. Internal oxidation occurred due to the formation of transient oxides during the initial oxidation period. These lower oxides allow anions to diffuse faster than cations, resulting in the formation of a mixed oxide layer with a predominance of Al and Cr along the inter-dendritic phase.

Figure 11 illustrates the oxide layer formed at 1000 ℃, which consists of a mixture of Al, Co, Cr, Cu, Fe, and Ni. The order of oxide layer formation aligns with the stability of oxide compounds as depicted in the Ellingham-Richardson diagram. Each layer is dominated by a particular oxide, with the order from lowest to highest stability being Al_2O_3, Cr_2O_3, spinel ((Co, Ni, Cu)(Al, Cr, Fe)$_2O_4$), a mixture of simple oxides (Fe_3O_4, CoO, NiO), and CuO. The Al_2O_3 layer was only partially formed due to Al depletion near the surface. Consequently, other elements are more likely to form oxides at a faster rate. At 1000 ℃, CuO formed in the upper layer due to the dominant presence of Cu in the inter-dendritic region. In contrast, Y. Y. Liu et al. [15] investigated the oxidation of $Al_xCoCrCuFeNi$ alloy at 1000 ℃ for 100 h and found that CuO oxide did not form in the outer layer of the oxide layer due to the poor adhesion properties of Cr_2O_3 oxide, which led to excessive exfoliation.

3.5 Oxidation Mechanism

The oxidation of the alloy can lead to the formation of a mixed oxide compound. When considering oxide formation, it is essential to account for the stability of the oxide-forming elements within the alloy. Several factors influence the kinetics of alloy oxidation, including the diffusivity of oxygen and the propensity of the alloying elements to react with oxygen. As a result, the oxides formed will exhibit varying growth rates, and the composition of the oxide at the metal/oxide interface will gradually change. The oxide with the highest concentration will ultimately dominate the growth of the oxide layer in that region.

Figure 12 illustrates the oxidation mechanism of the alloy at 800 and 900 ℃. The oxidation process begins with the interaction of oxygen with the substrate surface, where oxygen ions (anions) react with metal ions (cations) on the substrate. In the early stages of oxidation, a thin oxide layer or transient oxides, such as FeO, CoO, CuO, NiO, and spinel ((Co,Ni,Cu)(Al,Cr,Fe)$_2O_4$), forms on the metal surface. During exposure, oxygen diffuses through the transient oxide layer. According to the Ellingham-Richardson diagram, Cr and Al are the elements most likely to react under these conditions. This reaction leads to the formation of a Cr_2O_3 layer, which reduces the pO_2 within the substrate, facilitating the subsequent formation of an Al_2O_3 layer. The Al_2O_3 layer exhibits more stable properties at low oxygen activity. Both Cr_2O_3 and Al_2O_3 layers will thicken, further reducing the oxygen activity in the substrate.

As oxidation exposure time increases, an Al_2O_3 layer is anticipated to form uniformly and protectively on the alloy surface. However, the Al_2O_3 formed is a transient alumina (γ-Al_2O_3, δ-Al_2O_3, θ-Al_2O_3) that is less protective compared to α-Al_2O_3. This less protective nature allows for the diffusion of oxygen ions into the substrate through the oxide layer. If the oxygen content within the alloy exceeds its solubility limit, internal oxidation will occur beneath the oxide layer.

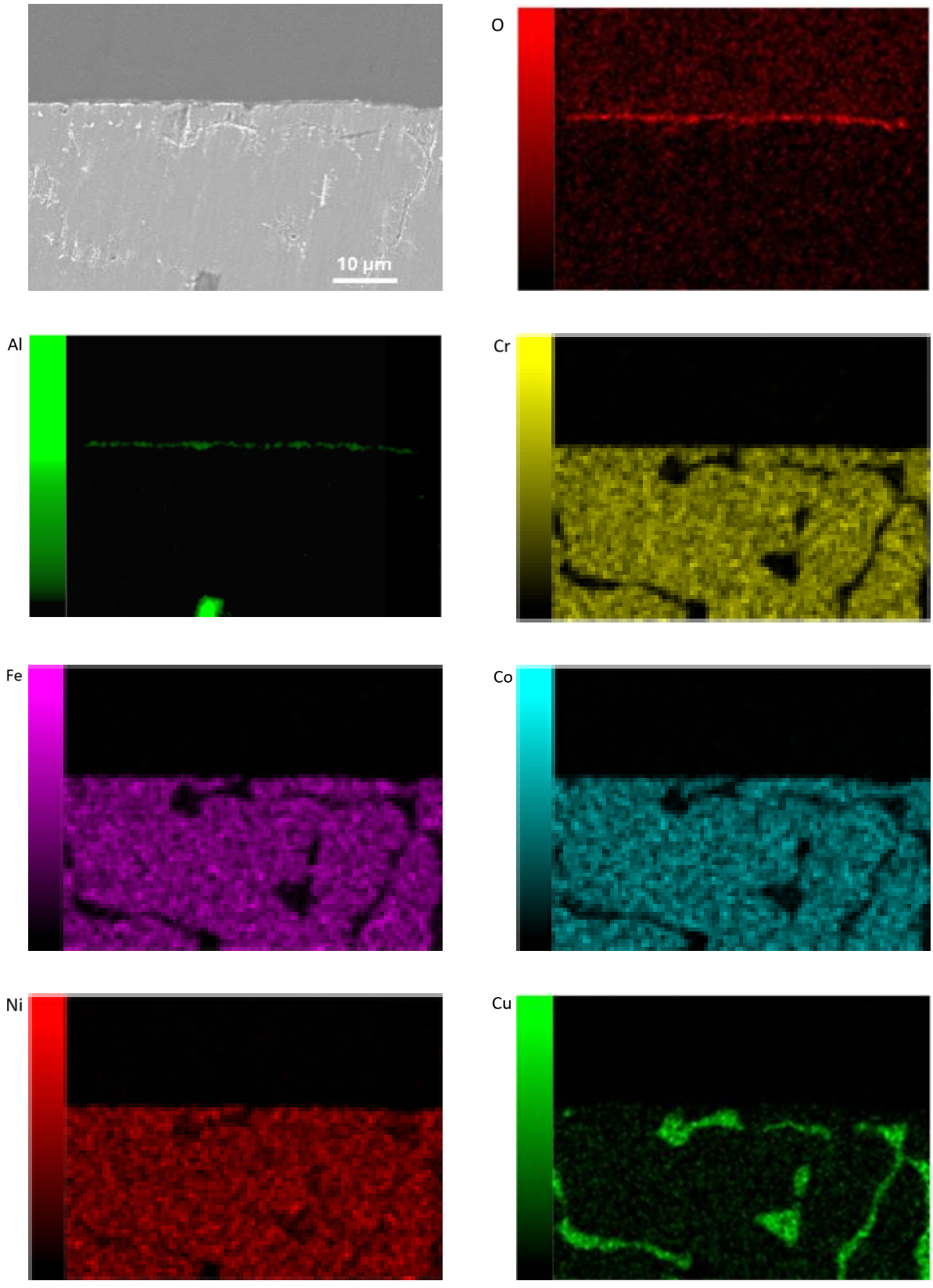

Figure 9. EDS mapping of cross-section sample at 800 °C for 2 h

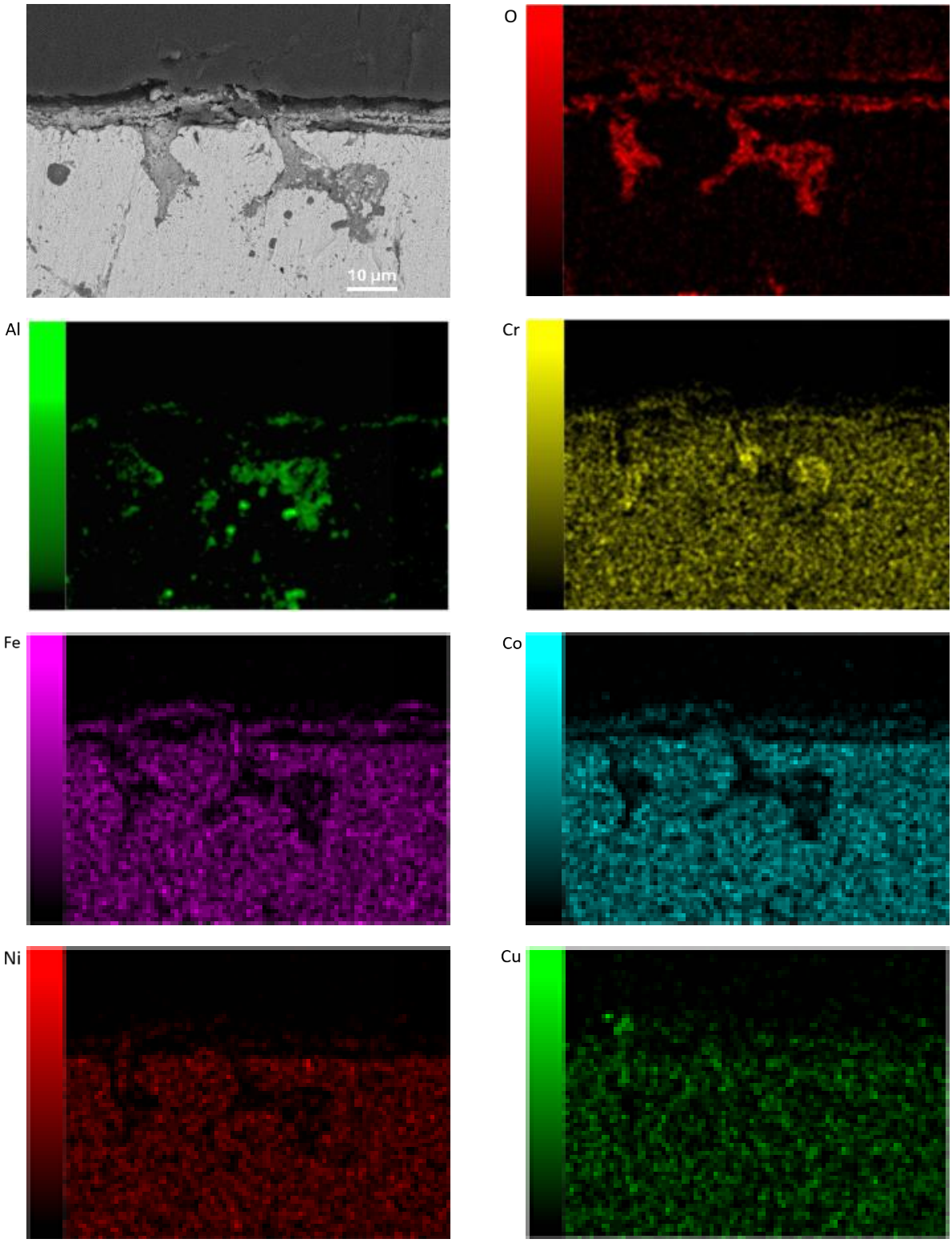

Figure 10. EDS mapping of cross-section sample at 900 °C for 2 h

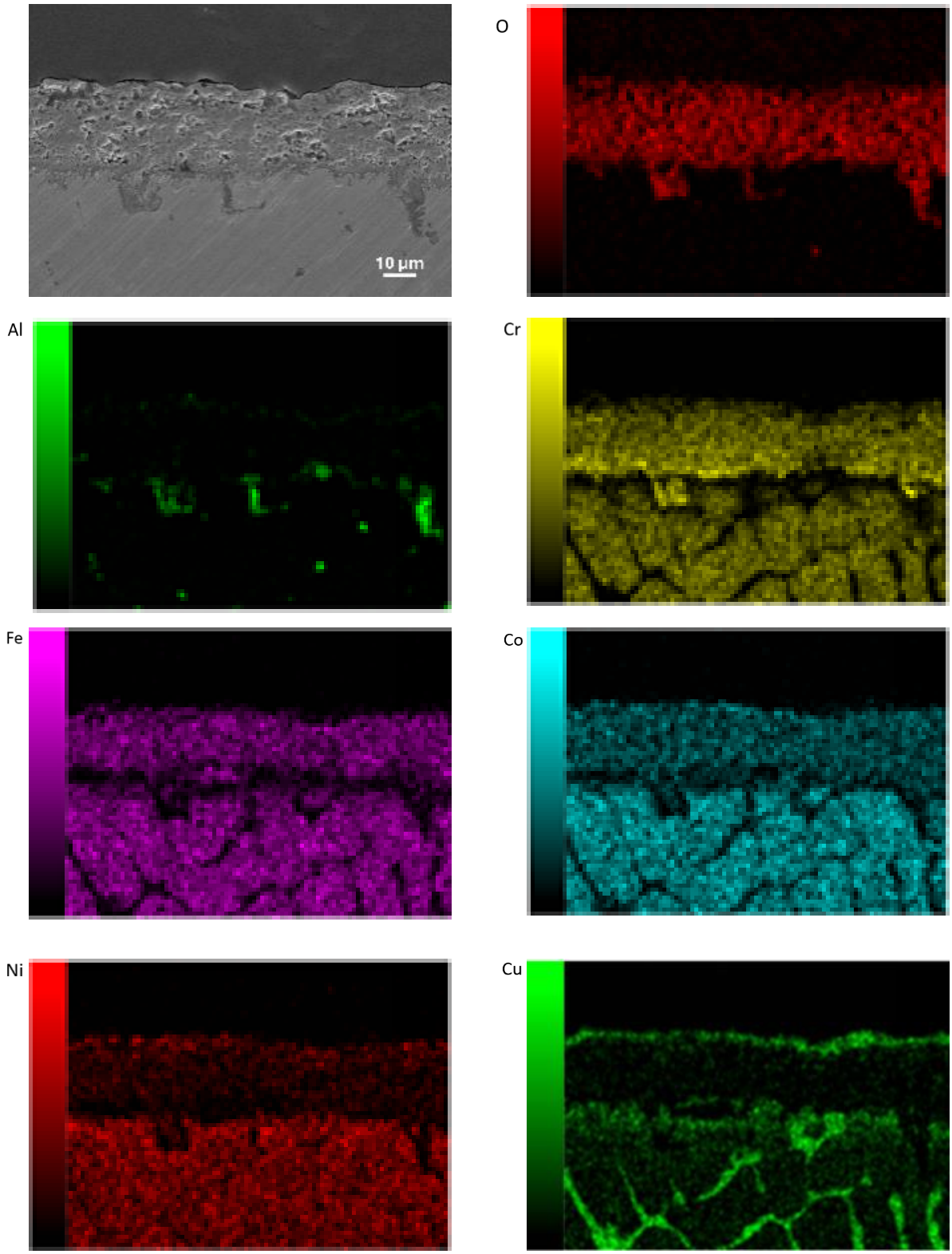

Figure 11. EDS mapping of cross-section sample at 1000 °C for 2 h

In this alloy, internal oxidation predominantly occurs along the inter-dendritic region, resulting in the formation of Al_2O_3 along with small amounts of Cr_2O_3 and CuO. Other elements will also form oxides, such as Fe_3O_4, CoO, CuO, NiO, and spinel ($(Co,Ni,Cu)(Al,Cr,Fe)_2O_4$). CuO oxide is formed on the surface of the oxide layer parallel to the inter-dendritic area due to the high Cu content in that region.

The oxidation mechanism of the $Al_{0.25}CoCrCuFeNi$ alloy at 1000 °C deviates from the previous mechanism due to the absence of a continuous Al_2O_3 layer, rendering it non-protective.

Initially, Cr_2O_3 forms during oxidation, followed by the formation of non-continuous Al_2O_3 due to Al depletion near the oxide/substrate interface.

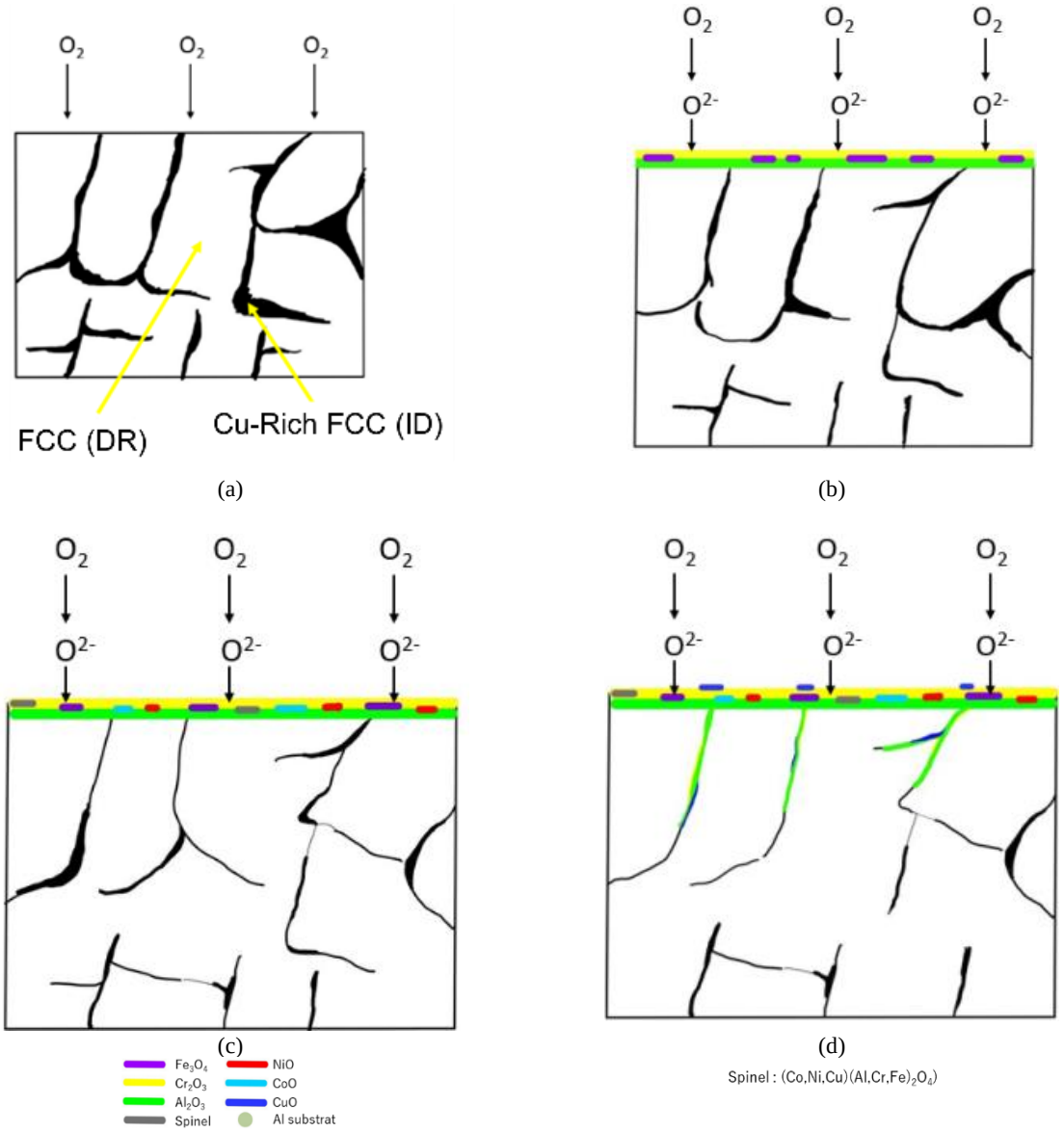

Figure 12. Illustration of oxidation mechanism of $Al_{0.25}CoCrCuFeNi$ alloy at 800 and 900 °C. (a) → (b) → (c) → (d)

This depletion is attributed to the slower diffusion rate of Al compared to other elements. The order of diffusion speed for elements from the lowest is as follows: Al, Cr, Ni, Co, and Fe. This sequence results in the formation of oxide layers such as Cr_2O_3, Fe_3O_4, CoO, NiO, and CuO, as well as spinel ($(Co,Ni,Cu)(Al,Cr,Fe)_2O_4$), on the outermost layer of the oxide scale.

CuO is formed in the outermost layer of the oxide layer in Cu-rich inter-dendritic areas. Consequently, the diffusion of Cu will occur extensively in multiple directions as illustrated in Fig. 13.

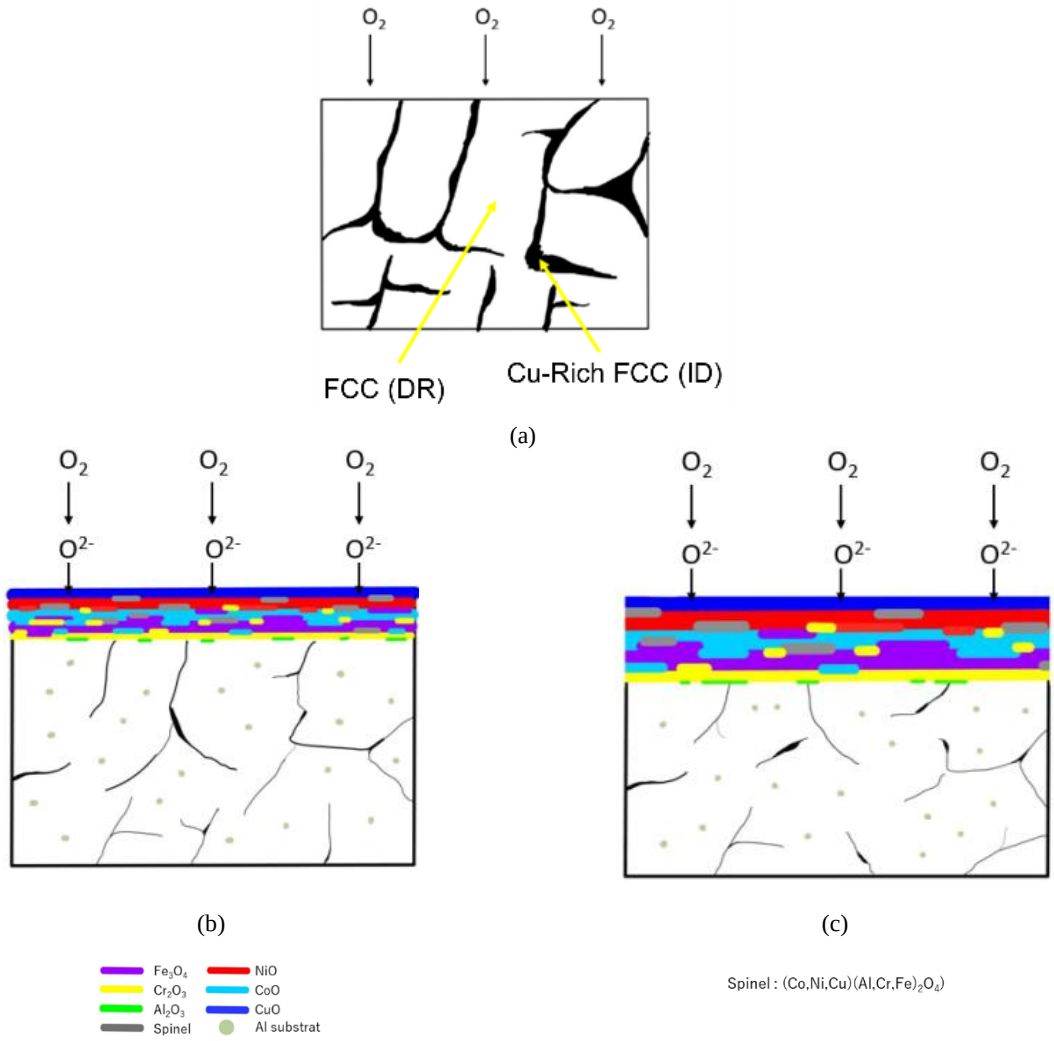

Figure 13. Illustration of oxidation mechanism of $Al_{0.25}CoCrCuFeNi$ alloy at 1000 °C. (a) → (b) → (c)

4. CONCLUSION

The oxidation behavior and microstructural evolution of the $Al_{0.25}CoCrCuFeNi$ HEA were examined at 800, 900, and 1000 °C for 2, 16, and 40 h. SEM-EDS confirmed that this alloy consists of an FCC phase in the dendritic region and a Cu-rich FCC phase in the inter-dendritic regions, consistent with the Hume Rothery rules and valence electron concentration value. The oxides formed during the oxidation process include Al_2O_3, Cr_2O_3, Fe_3O_4, CoO, CuO, NiO, and spinel oxides $(Co,Ni,Cu)(Al,Cr,Fe)_2O_4$), with distinct formation mechanisms at a temperature below 900 °C compared to those at or above 1000 °C. All types of Al_2O_3 formed were transient oxides, with variations such as γ-Al_2O_3, δ-Al_2O_3, and θ-Al_2O_3 at 800, 900, and 1000 °C, respectively.

ACKNOWLEDGMENT

This research was funded by the Program Riset dan Inovasi untuk Indonesia Maju (RIIM) Gelombang 2 the National Research and Innovation Agency (BRIN) and Educational Fund Management Institution (LPDP), grant number 78/IV/KS/11/2022 and 834/IT1.B07/KS.00/2022 which is greatly acknowledge.

REFERENCES

[1] A. Turchi, D. Bianchi, F. Nasuti, and M. Onofri, "A numerical approach for the study of the gas–surface interaction in carbon–phenolic solid rocket nozzles," *Aerosp Sci Technol*, vol. 27, no. 1, pp. 25-31, 2013. Doi: 10.1016/j.ast.2012.06.003.

[2] C. Katsarelis, P. Chen, P. Gradl, C. Protz, Z. Jones, D. Ellis, and L. Evans, "Additive manufacturing of NASA HR-1 material for liquid rocket engine component applications," *JANNAF Dec*, p. https://ntrs.nasa.gov/search.jsp?R=20200001007, 2019. [Online]. Available: https://ntrs.nasa.gov/api/citations/20200001007/downloads/20200001007.pdf%0Ahttps://ntrs.nasa.gov/search.jsp?R=20200001007

[3] Md. Shahwaz, P. Nath, and I. Sen, "A critical review on the microstructure and mechanical properties correlation of additively manufactured nickel-based superalloys," *J Alloys Compd*, vol. 907, pp. 164530, 2022. Doi: 10.1016/j.jallcom.2022.164530.

[4] T. M. Pollock and S. Tin, "Nickel-based superalloys for advanced turbine engines: Chemistry, microstructure and properties," *J Propuls Power*, vol. 22, no. 2, pp. 361-374, 2006. Doi: 10.2514/1.18239.

[5] W. Xia, X. Zhao, L. Yue, and Z. Zhang, "A review of composition evolution in Ni-based single crystal superalloys," *J Mater Sci Technol*, vol. 44, pp. 76-95, 2020. Doi: 10.1016/j.jmst.2020.01.026.

[6] Y. Zhang, T. T. Zuo, Z. Tang, M. C. Gao, K. A. Dahmen, P. K. Liaw, and Z. P. Lu, "Microstructures and properties of high-entropy alloys," *Prog Mater Sci*, vol. 61, pp. 1-93, 2014. Doi: 10.1016/J.PMATSCI.2013.10.001.

[7] J. W. Yeh, "Recent progress in high-entropy alloys," *Annales de Chimie: Science des Materiaux*, vol. 31, no. 6, pp. 633-648, 2006. Doi: 10.3166/acsm.31.633-648.

[8] T. Wang, W. Jiang, X. Wang, B. Jiang, C. Rong, Y. Wang, J. Yang, and D. Zhu, "Microstructure and properties of Al0.5NbTi3VxZr2 refractory high entropy alloys combined with high strength and ductility," *Journal of Materials Research and Technology*, vol. 24, pp. 1733-1743, 2023. Doi: 10.1016/J.JMRT.2023.03.103.

[9] D. B. Miracle and O. N. Senkov, "A critical review of high entropy alloys and related concepts," *Acta Mater*, vol. 122, no. October, pp. 448-511, 2017. Doi: 10.1016/j.actamat.2016.08.081.

[10] J. Lu, G. Ren, Y. Chen, H. Zhang, L. Li, A. Huang, X. Liu, H. Cai, X. Shan, L. Luo, X. Zhang, and X. Zhao, "Unraveling the oxidation mechanism of an AlCoCrFeNi high-entropy alloy at 1100 °C," *Corros Sci*, vol. 209, pp. 110736, 2022. Doi: 10.1016/J.CORSCI.2022.110736.

[11] T. M. Butler and M. L. Weaver, "Oxidation behavior of arc melted AlCoCrFeNi multi-component high-entropy alloys," *J Alloys Compd*, vol. 674, pp. 229-244, 2016. Doi: 10.1016/j.jallcom.2016.02.257.

[12] T. M. Butler, M. J. Pavel, and M. L. Weaver, "The effect of annealing on the microstructures and oxidation behaviors of AlCoCrFeNi complex concentrated alloys," *J Alloys Compd*, vol. 956, pp. 170391, 2023. Doi: 10.1016/j.jallcom.2023.170391.

[13] S. Guo, C. Ng, J. Lu, and C. T. Liu, "Effect of valence electron concentration on stability of fcc or bcc phase in high entropy alloys," *J Appl Phys*, vol. 109, no. 10, 2011. Doi: 10.1063/1.3587228.

[14] A. Takeuchi and A. Inoue, "Calculations of mixing enthalpy and mismatch entropy for ternary amorphous alloys," *Materials Transactions, JIM*, vol. 41, no. 11, pp. 1372–1378, 2000. Doi: 10.2320/matertrans1989.41.1372.

[15] Y. Y. Liu, Z. Chen, Y. Z. Chen, J. C. Shi, Z. Y. Wang, S. Wang, and F. Liu, "Effect of Al content on high-temperature oxidation resistance of AlxCoCrCuFeNi high entropy alloys (x=0, 0.5, 1, 1.5, 2)," *Vacuum*, vol. 169, pp. 108837, 2019. Doi: 10.1016/J.VACUUM.2019.108837.

[16] J. Lee, H. Jeon, D. G. Oh, J. Szanyi, and J. H. Kwak, "Morphology-dependent phase transformation of γ-Al_2O_3," *Appl Catal A Gen*, vol. 500, pp. 58-68, 2015. Doi: 10.1016/J.APCATA.2015.03.040.